Gas Processing Journal

Vol. 10, No. 2, 2022, pp. 53 - 64
http://gpj.ui.ac.ir

Research Paper

Proposing a ceramic-based nanofiltration system to capture nanoparticles used in the gas processing industry

Hamid Talebi [1], Hossain Nemati [*1], Ehsan Selahi [1]

[1] Department of Mechanical Engineering, Marvdasht Branch, Islamic Azad University, Marvdasht, Iran

Received: 2023-07-19 Revised: 2023-09-23 Accepted: 2023-11-21

Abstract: In this study, a numerical analysis of different types of ceramic coating methods for a modified nanoparticle filtration system is investigated. The novelty of this study is based on proposing a nanofiltration model assisted by ceramic-based coating, leading to less energy consumption during the filtration process. The fluid velocity entering the nanofiltration system ranges from 20 to 75 m/s. Key parameters are identified and evaluated to assess the impact of energy losses on system performance. The results indicate that as the fluid velocity increases, both the pressure on the filter and the force on the system increase. The increase in shear stress on the wall also leads to an increase in the kinetic energy of the fluid, which can affect its turbulence. Three types of coatings, namely SiO2, Sic, and Si3N4, were examined. The use of SiO2 coating resulted in a 21% decrease in temperature compared to the case without coating, thus reducing energy losses. The optimal coating thicknesses were found to be 1 mm for SiO2, 1.2 mm for SiC, and 1.4 mm for Si3N4. The results show that using SiO2 coating can reduce energy losses by 19.34%. The pressure in the middle side of the filtration system is the highest due to the accumulation of nanoparticles, reaching a maximum value of 160 kPa. Conversely, the pressure in the corners of the filtration system is the lowest, with a value of 95.13 kPa.

keywords: Nanoparticle, Nanofiltration, Coating, Ceramic-based, Energy

1- Introduction

Nanofiltration is a device that operates on a selectively permeable membrane. The term "nanofiltration" refers to the filtration of particles on a nanometer scale, allowing the separation of substances based on their molecular size and charge. Unlike other membrane processes, nanofiltration offers intermediate selectivity, positioned between reverse osmosis and ultrafiltration, making it highly versatile (Yadav et al. 2022). Nanofiltration membranes have been found to effectively remove various contaminants present in gas streams, including acidic gases like carbon dioxide and hydrogen sulfide. These pollutants, when released into the atmosphere, contribute to climate change and air pollution.

In recent years, with the development of nanotechnology, the use of nanomaterials in various industries and products has increased. This has led to an increase in the release of these substances into the environment. In addition, nanoparticles (as materials with three external dimensions at the nanoscale, under 100 nm) can cause adverse effects on the environment due to their unique physical properties (Cha et al. 2022). Nano-fluid is a fluid with at least one component in the size range of 1 to 100 nm. Sample nanoparticles can be metals, metal oxides, carbides, or fullerenes. These nanoparticles affect the desired properties of the fluid, such as increasing the thermal conductivity, increasing the tribological effects, and increasing the chemical advances. The surface of nanoparticles may play a major role in these effects with the chemical surface (Weyd et al. 2021). Nanoparticles can be mainly divided into hydrophilic and petroleum particles (Kashiwada 2006). Today, due to the increasing price of fossil fuels and the expiration of these fuels, any activity in reducing energy consumption is very valuable. The filtration system is used to remove contaminants from the fluid mixture. Preliminary toxicology studies have shown that nanoparticles can affect human health and have environmental effects. Inhalation of aerosol particles has been identified as a threat to our respiratory health (Kreyling et al. 2002). Meanwhile, Thongyen et al. (2015) used a sample of a laser filter using TEM networks as an internal mesh plate and sampling was performed successfully. It seems that the combined use of mesh and impactor screens can be used as a desirable separator for

* Corresponding Author.
Authors' Email Address: [1] H. Talebi (hamidtalebi1970@hotmail.com), [2] H. Nemati (hossainnemati@hotmail.com), [3] E. Selahi (ehsanselahi@hotmail.com)

http://dx.doi.org/10.22108/GPJ.2023.137639.1129

nanoparticle filtration in various applications. In this regard, the research of Zhang et al. (2017) proposed a hybrid model of a lattice plate and an impactor as a new separation tool for aerosol nanoparticle separation. Shah et al. [30] compared centrifugation and tangential flow filtration for purifying acetylated dextran nanoparticles. This study aimed to investigate the effect of various factors on the characteristics of pure nanoparticles (NPs) using TFF. Lee et al. (2017) investigated liquid filtration of nanoparticles through membrane filters under adverse conditions and different ion strength conditions. Kefayati (2015) simulated the effect of a magnetic field on FDLBM on composite convection in a two-way covered cavity filled with non-Newtonian nanofluid. In this study, laminar composite convection of non-Newtonian nanofluids in a two-way indoor exposure in the presence of a horizontal magnetic field was analyzed using FDLBM. Landfahrer et al. (2017) investigated a numerical model of computational fluids to predict the transient temperature distribution of the transfer and rotational motion of pipes in a gas-fired furnace. Sheikholeslami and Rokni (2017) numerically simulated the natural convective conductivity of nanofluid in a half-ring in the presence of Lorentz force. In that study, the effect of an external magnetic field on the heat transfer of fluoride in a cavity with a circular hot wall was reported. Hayat et al. (2017) studied numerical modeling of non-Newtonian fluids and presented a new formula and results. They referred to the flow of the CARREAU fluid magnetic hydrodynamic stagnation point in the presence of homogeneous-heterogeneous reactions. In their study, Barnoon and Toghraie (2018) numerically investigated the multilayer flow modulation and heat transfer of non-Newtonian nanofluids in a porous medium. In that study, a comprehensive study of the laminar flow and heat transfer of a quasi-plastic non-Newtonian nanofluid within the porous region of concentric circles was presented.

Much research has been conducted to study the coating of nanofiltration in recent years. Chen et al. (2022) created an interfacial coating interlayer on an ultrafiltration substrate using glutaraldehyde to crosslink polyethyleneimine and dextran nanoparticles. The interlayer improved membrane density and prevented selective defects associated with the incorporation of nanoparticles. The interlayered- thin film composite nanofiltration membrane had a pure water permanence of four times that of the pristine membrane, and improved retention rates for various divalent salts, with Na2SO4 exceeding 98%. This interlayer modification method has the potential for rapid desalination and wastewater recovery, offering new possibilities for high-performance ultrafiltration membranes in industrial applications. More materials can studied for coating of nanofiltration compared with the work of Chen et al. (2022). In the work of Jiang et al (2022), a nanofiltration membrane was created by coating a polyvinylidene fluoride substrate with tannic acid and polydopamine. The resulting membrane was analyzed using various techniques to determine its properties. The modified membrane was found to have increased surface roughness and hydrophilicity with higher concentrations of tannic acid. The membrane was stable during the separation process and had a higher permeating flux compared to other similar studies. This suggests that the modified membrane could be useful in industrial applications for separating dye wastewater. They studied the effect of heating time on the temperature of the coating layer. A study was conducted by Chen et al. (2023) to create a modified nanofiltration membrane by coating a substrate with tannic acid and Silicon dioxide (SIO2). The resulting membrane had increased hydrophilicity and surface roughness with higher tannic acid concentrations and demonstrated high rejection rates for various dyes and superoleophobic properties. It was stable during the separation process and had a higher permeating flux compared to other similar studies, making it suitable for industrial applications in separating dye wastewater. By optimizing a simple one-step fabrication process, the performance of the composite nanofiltration membranes was greatly improved, making it a promising method for developing high-performance membranes.

So far, few studies have investigated the heat transfer in particle filtration under three-dimensional flow and the effect of system coating on losses of the filtration system. Therefore, to fill this gap, this research has been conducted. In this study, numerical analysis of heat transfers and ceramic coatings using the CFD method in ANSYS software is carried out by modeling the particle filtration system in both adiabatic and non-adiabatic modes. The influence of parameters such as fluid velocity ranging from 20 to 75 m/s, filter pressure, wall shear stress, fluid kinetic energy, and force on fibers is examined to evaluate the effect of losses on system performance. The effect of three different types of insulation coatings on the wall of the system is examined to minimize heat transfer, and the optimal thicknesses are determined.

2- Methods

GAMBIT and CATIA V5 software are used to simulate the initial model, and then the initial geometry is transferred to ANSYS software for flow analysis and filtration evaluation. The analytical model of this research is based on solving the momentum equations, and the equations related to pressure and velocity are simultaneously examined and calculated in an integrated system. These calculations are performed by discretizing relations in a similar step to when the ANSYS software solver performs these calculations. The fluid flow is considered to be compressible so that the effect of the axial velocity of the nanoparticles, which causes a sharp increase in flow velocity within it, can be utilized. Additionally, the turbulence model used is of the standard k-ε type. In this study, due to the complex geometry, the finite element method (FEM) based on the work of Gozálvez-Zafrilla and Santafé-Moros (2010) has been employed. The numerical solution of the equations governing flow and heat transfer for the base fluid under standard conditions yields a velocity and pressure field within the filter medium. The obtained data are used to determine the key parameters of the filter, the numerical solution of the nanoparticle mass transfer equation, and the extraction of results from a Lagrange perspective. The results show that the key parameters of a woven filter are fiber diameter, compression ratio, number of fibers, and filter thickness.

2-1 Boundary specifications and conditions

Table (1) presents the characteristics of the woven filter studied in this research. Table 2 presents the flow simulation boundary conditions in three-dimensional mode.

Table 1 Specifications of the woven filter used in the present study

Parameter	Value
Number of fibers	**36**
Diameter of fiber	**4 mm**
Length of fiber	**30 mm**
Density Percentage	**15 %**
Nanoparticle Concentrate	**25 nm in the base fluid**
Density of nanoparticles	**1000 Kg/ m^3**
Thermal conductivity	**1.1 W/K**
Thermal capacity at constant pressure	**800 J/Kg K**

Table 2 Simulation boundary conditions in the 3D mode

Parameter	Value
Temperature	**298.15 K**
Inlet Pressure	**101.3 KPa**
Inlet Velocity	**0.1 m/s**
Outlet Pressure	**1 atm**

Periodic boundary conditions are used for the upper and lower boundaries. The choice of periodic lateral boundary conditions is due to the fact that part of the filter is modeled here and the filter environment will be repeated at the upper and lower boundaries.

2-2 Validation

Validation of the base model is obtained compared with that of the work of Lim et al. (2017) as shown in Figs. 1 and 2. A comparison of the results shows that the model used in this study is confirmed. Fig. 1 shows the penetration value against the mobility diameter (D_m) for fibrous filter, Fig. 2 is obtained for the screen filter which is similar to the model used as final case in thus study.

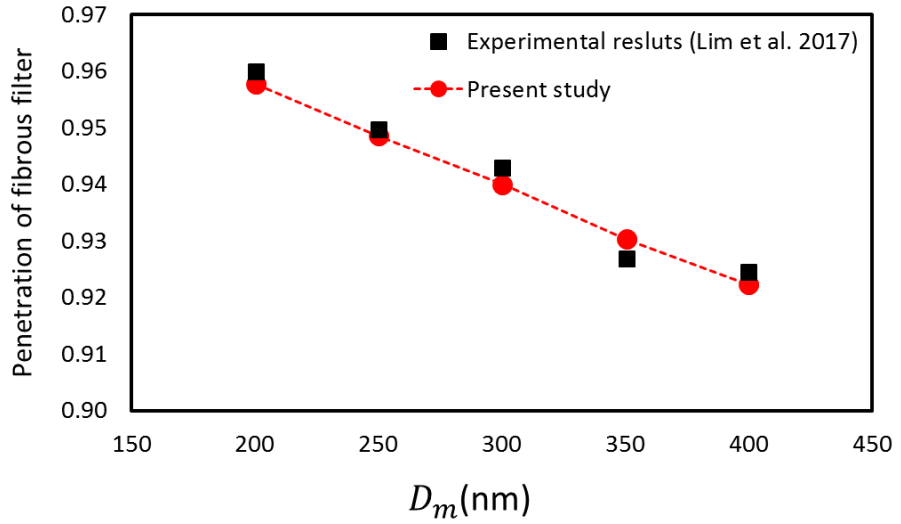

Fig. 1 Validation of penetration of the initial model for screen compared with that of Lim et al. (2017).

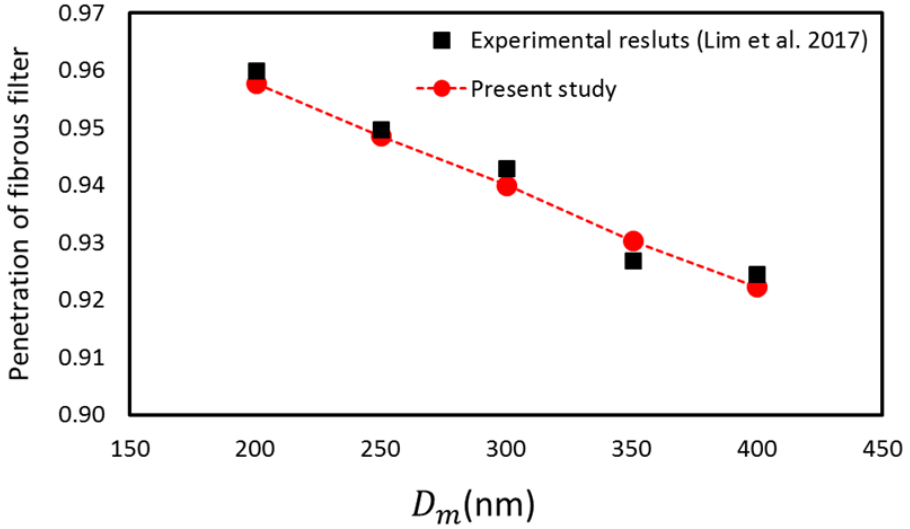

Fig. 2 Validation of penetration of the initial model for screen filter compared with that of Lim et al. (2017).

2-3 Assumptions

Fig. 3 shows the mesh convergence diagram, as can be seen, the mesh number of 46737 is determined as the convergence point. In the present study, the nanoparticle fluid mixture behaves as a two-component mixture (air-based fluid and solid nanoparticles) with the following hypotheses (Lim et al. 2017):

- The fluid flow is incompressible.
- Steady-state conditions are assumed.
- A state of no chemical reaction is considered.
- The effect of external forces is negligible and volumetric forces are omitted.
- There is no heat source in the environment.
- Radiant heat transfer can be neglected.
- Nanoparticles in thermal equilibrium with the base fluid.
- The motion of nanoparticles due to the motion of the fluid is a one-way connection point and is the basis.

If the fiber diameter is greater than 10 micrometers, the Knudsen number of fibers is less than 0.001. In this case, the flow regime is continuous around the fibers, and within this regime, the Navier-Stokes equations can be used to analyze the flow behavior of the base fluid. Also, the Knudsen number for nanoparticles is $0.1 < Kn_p < 10$, which is in the transient flow regime. In this case, the flow around the nanoparticles will be discontinuous. Fig. 4 shows the fiber model.

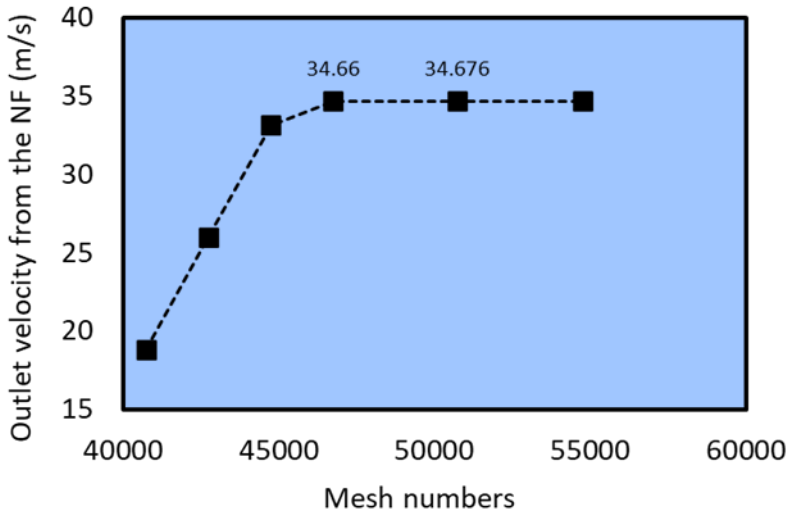

Fig. 3 Mesh convergence analysis

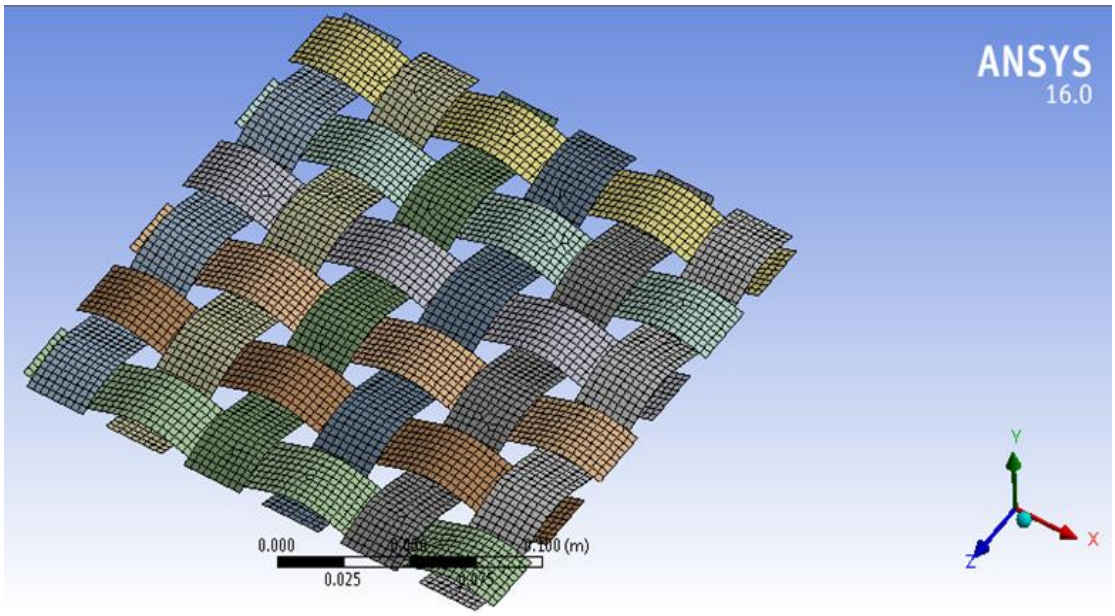

Fig. 4 Proposed model of the nanoparticle filtration

2-4 Strengths and Limitations

The advantage of using a coating on nanofiltration is to increase its lifespan compared to the uncoated state, which reduces the secondary costs associated with nanofiltration. This is because the thermal resistance of the nanofiltration process, aided by the coating, increases to withstand high temperatures. However, ceramic coating is more expensive compared to other types of coatings. However, a commercially available porous channel monomer module provides a more cost-effective solution compared

to using a single tubular membrane module. This is because it increases the surface area of each membrane within a given volume, reduces labor costs associated with coating the membrane layer, and simplifies the module structure, thereby reducing mechanical costs (Chen et al. 2022).

3 Methods

The basic principle used in fluid mechanics is the principle of mass conservation. This principle states that mass is neither produced nor eliminated and is expressed by the continuity equation for compressible and non-compressible fluids (Razavi et al 2020):

$$\frac{\partial \rho}{\partial t} + \vec{\nabla}.\left(\rho \vec{V}\right) = 0 \quad (1)$$

$$\left(\vec{\nabla}.\vec{V}\right) = 0 \quad (2)$$

Fluid mechanics is not only determined by the equation of continuity but also by the principle of survival of motion or Newton's second law. The magnitude of motion is the product of mass in velocity. Newton's second law states that the result of the forces acting on an object is equal to the net momentum change. Considering the incompressible flow and assuming a constant viscosity coefficient, the form of the Navier-Stokes equation is as follows (Lin et al. 2022 and Faramarzi et al. 2021):

$$\rho \frac{DV}{Dt} = \rho f - \nabla P + \mu \nabla^2 V \quad (3)$$

Where V is the velocity vector, P is pressure, f is volume force and μ is viscosity. $\frac{D}{Dt}$ is a material derivative and is defined as $\left(\frac{D\varphi}{Dt} = \frac{\partial \varphi}{\partial x} + \vec{V}, \nabla \varphi\right)$ [13]. For compressible flow, the continuity equation for turbulent flow is as follows (Lin et al. 2022):

$$\frac{\partial}{\partial x_i}(\overline{\rho\, u_i}) + \frac{\partial}{\partial x_i}(\overline{\rho'\, u_i'}) = 0 \quad (4)$$

For incompressible flow, $\rho' = 0$, therefore the above equation is as follows:

$$\frac{\partial \bar{u}_i}{\partial x_i} = 0 \quad (5)$$

Momentum equation for turbulent flow is as follows (Lin et al. 2022):

$$\rho\left[\frac{\partial \bar{u}_i}{\partial t} + \bar{u}_j \frac{\partial \bar{u}_i}{\partial x_j}\right] = \bar{B}_i - \frac{\partial \bar{p}}{\partial x_i} + \frac{\partial}{\partial x_j}\left[\mu \frac{\partial \bar{u}_i}{\partial t} - \rho \overline{u_i' u_j'}\right] \quad (6)$$

The only difference between the above equation and the momentum equation is the moment quantities added to the last expression to the right of the equation $\rho \overline{u_i' u_j'}$.

This term is called perturbation stress or Reynolds stress. In order to consider the wall function, experimental formulas are used that use the interaction between the viscosity of the substrate area and the boundary conditions close to the wall to make the relationship between the equilibrium velocity equations and the turbulence transfer. The mentioned method is based on the work of Cheng et al. (1990). In this method, it is assumed that the shear stress of the wall is located within the boundary layer of the area which is completely turbulent. The velocity equation near the wall is determined by the following equations (Lim et al. 2017):

$$u^+ = \frac{1}{\kappa} ln y^+ + C \quad (6)$$

$$y^+ = \frac{\rho \Delta y\, u_\tau}{\mu} \quad (7)$$

$$u_\tau = \left(\frac{\tau_w}{\rho}\right)^{1/2} \quad (8)$$

According to studies, the value of the wall function around the wall is not less than 11.36 physically. Values greater than 200 also cause vortices in the boundary layer, which indicates that the networking is unsuitable and large (Lim et al. 2017). Therefore, the optimal value for the wall function is in the range of 11.36 and 200. As mentioned earlier, the predominant forces on the particles are the base fluid drag force and the Brownian and Thermophoresis forces. For particles when the Reynolds number is less than one, the following equations are considered (Lim et al. 2017):

$$\frac{du_p}{dt} = \frac{18\mu}{\rho_p d_p^2 C_c}\left(u - u_p\right) - \frac{3\pi\mu^2 d_p H}{\rho_a T}\nabla T + G_i \sqrt{\frac{\pi 216 v k_B T}{\pi \rho_p d_p^5 S^2 C_C \Delta t}} \quad (9)$$

$$\frac{dv_p}{dt} = \frac{18\mu}{\rho_p d_p^2 C_c}\left(v - v_p\right) - \frac{3\pi\mu^2 d_p H}{\rho_a T}\nabla T + G_i \sqrt{\frac{\pi 216 v k_B T}{\pi \rho_p d_p^5 S^2 C_C \Delta t}} \quad (10)$$

$$H \cong \left(\frac{2.34}{1 + 6.84\frac{\lambda}{d_p}}\right)\left(\frac{\frac{k}{k_p} + 4.36\frac{\lambda}{d_p}}{1 + 2\frac{k}{k_p} + 8.72\frac{\lambda}{d_p}}\right) \quad (11)$$

v ،p ،T and C are components of velocity with dimension in direction and perpendicular to flow, pressure with dimension, temperature with dimension, nanoparticle concentration, and μ ،k ،ρ ،λ , k_d are dynamic viscosity, heat conduction coefficient, density, and average free scan length are the basic fluid molecules and Boltzmann constant, respectively. The Cunningham slip correction coefficient on the surface of nanoparticles is as follows (Hosseini and Tafreshi 2010).

$$C_c = 1 + \frac{\lambda}{d_p}\{1.257 + 0.4\exp(-\frac{1.1d_p}{\lambda}) \quad (12)$$

4 Results

In this problem, the transient method is used. Also, because the composition of the fluid (air) is incompressible, we use the pressure-based method. To investigate the turbulent flow, the standard $k-\epsilon$ model is utilized, with its specifications presented in Table 3. The momentum and continuity equations are used for the simulation. Additionally, the input conditions are considered as "speed input" and its output as "output pressure". It should be noted that the velocity of the fluid at the filtration inlet is 30 m/s and the pressure at the outlet is 101325 Pa. Table 4 provides specifications for flow viscosity, showing the fluid characteristics and general conditions in this study.

Table 3 Flow viscosity characteristics

Viscosity Model	$k-\varepsilon$
$k-\varepsilon$ model	***Realizable***
C2 (epsilon)	**1.9**
Prandtl Number (TKE)	**1**
Prandtl Number (TDR)	**1.2**

Table 4 Fluid specifications and general conditions of the problem

Parameters	**Value**
Density (Kg/m^3)	**1.225**
Viscosity (Kg/s)	1.7894×10^{-5}
Temperature (K)	**288.16**
Velocity (m/s)	**45**
Special heat rate	**1.4**
Enthalpy (J/kg)	**0**
Inlet Pressure (Pa)	**0**

Nanoparticles used in this research are clay type and in standard conditions, they have a density of 1000 kg /m3 and a thermal conductivity of 1.1 W/K .To solve different equations from the "Simple" algorithm and also for discretization, the equations are selected second-order so that the confusion and results are more accurate. Finally, set the solution time step to 0.00015 seconds (350 repetitions) and set the convergence error rate at 1×10^{-6}. Finer meshes increase the analysis time as well as the accuracy of the analysis. But it is not affordable. Larger meshes drastically reduce analysis time but also cause severe errors due to sequential simplifications. On the other hand, the size of the grid sometimes will not affect the solution of the model, and the smaller size only increases the solution time. Under the same conditions, the mass flow rate is calculated for different grid sizes (Tang et al. 2016). In order to determine the appropriate mesh, in addition to using the above criteria, the independence of the solution from the number of meshes is examined as shown in Table 5. The results of the flow rate value are shown based on the change in the number of the meshes used in the modeling provided in Table 5. As can be seen, from the fourth mode onwards, the value of the output flow velocity continues at a steady trend, which can be concluded that the final grid of the model has 12807 nodes and 46735 elements. By applying the boundary conditions and applying the governing equations in the next step, the system is simulated and analyzed. In the final grid network, the minimum quality of the meshes is 0.193 and the highest aspect ratio is 19.2789.

Table 5 Comparison of mesh independence analysis

Nodes number	**Outlet flow rate from filtration (m/s)**
8563	**10.257**
10356	**18.793**
11748	**25.981**
12807	**34.66**
13500	**34.67**
15000	**34.675**

Fig. 5 shows changes in shear stress on the wall around the filtration at a fluid velocity of 30 m/s. As can be seen, the maximum amount of stress occurs at the beginning of filtration, which is 125.6 Pa. The lowest value of stress is found at a lower level and output, measuring 0.000009482 Pa. On the other hand, Fig. 6 investigates shear stress in the filtration section. As can be seen, the maximum amount of shear stress is 14.01 Pa and the lowest value is -1.1402 Pa, which is lower than that on the wall around the filtration system.

Figs. 7 and 8 show the compressive force on the wall around the filtration system and the filtration itself, respectively. Based on the results, it is observed that the pressure differences across the model are close to each other, which is due to the velocity of the fluid entering it. On the other hand, because the fibrous surface of the filtration is considered to be somewhat small, this pressure is increased due to the increase of the aerodynamic forces of the fluid. According to the Figs. 7 and 8, it can be seen that the pressure in the middle of the filtration due to the accumulation of nanoparticles has the highest value of 1.602×10^5 Pa, while the pressure in the filtration corners has the lowest value of $0.9513 \times 10^{+5}$ Pa.

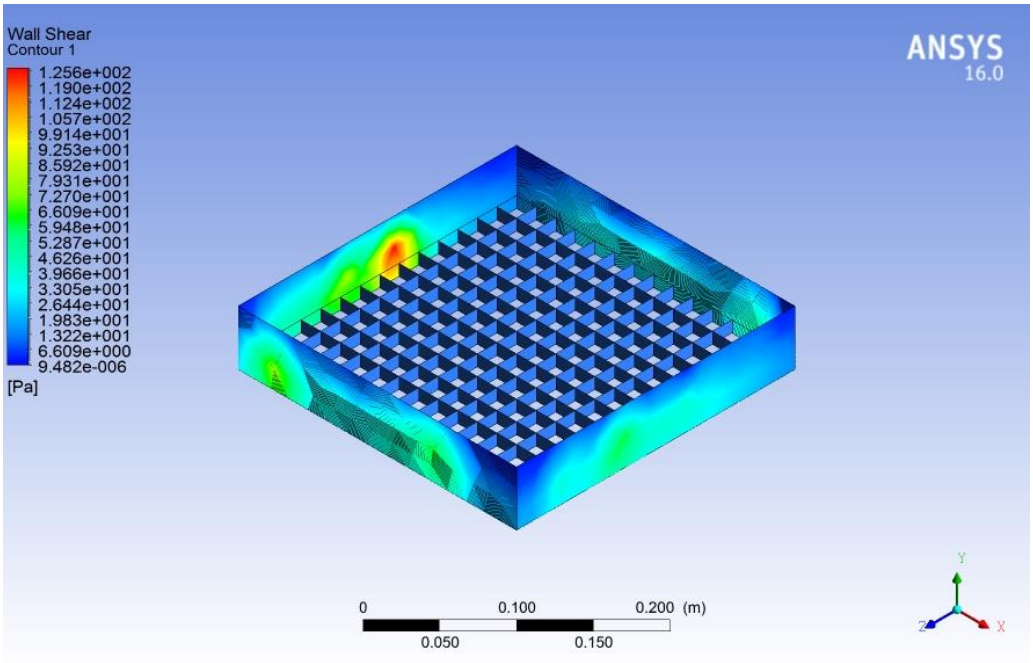

Fig. 5 The shear stress on the wall around the filtration

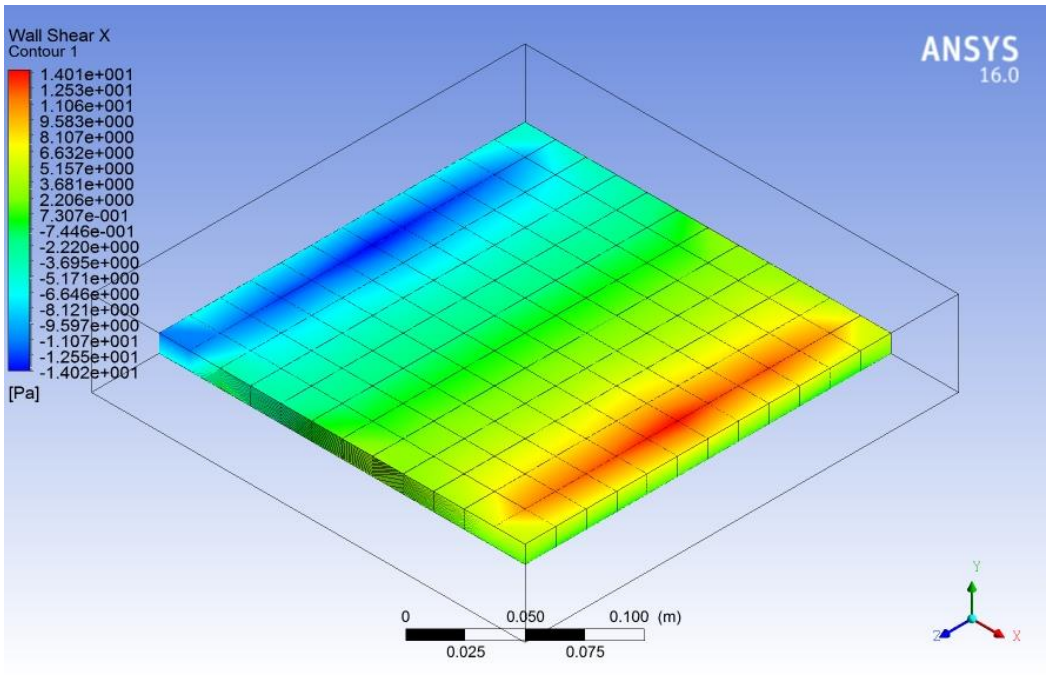

Fig. 6 Shear stress on the filtration wall

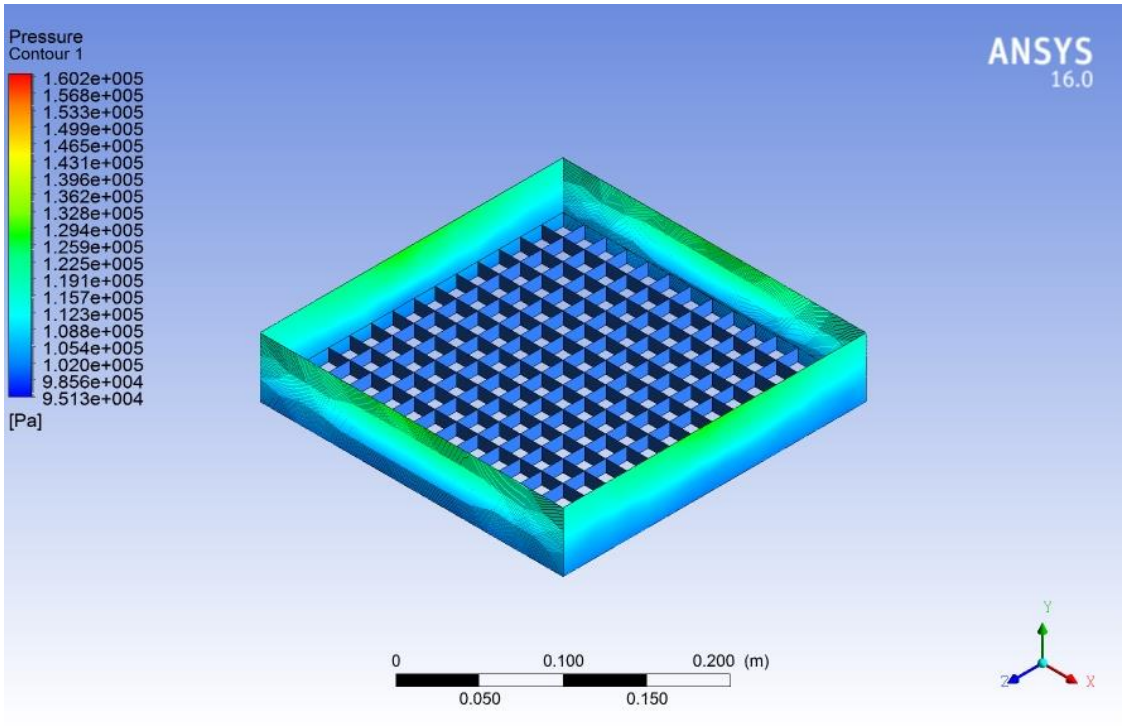

Fig. 7 Pressure variation on the wall around the filtration system.

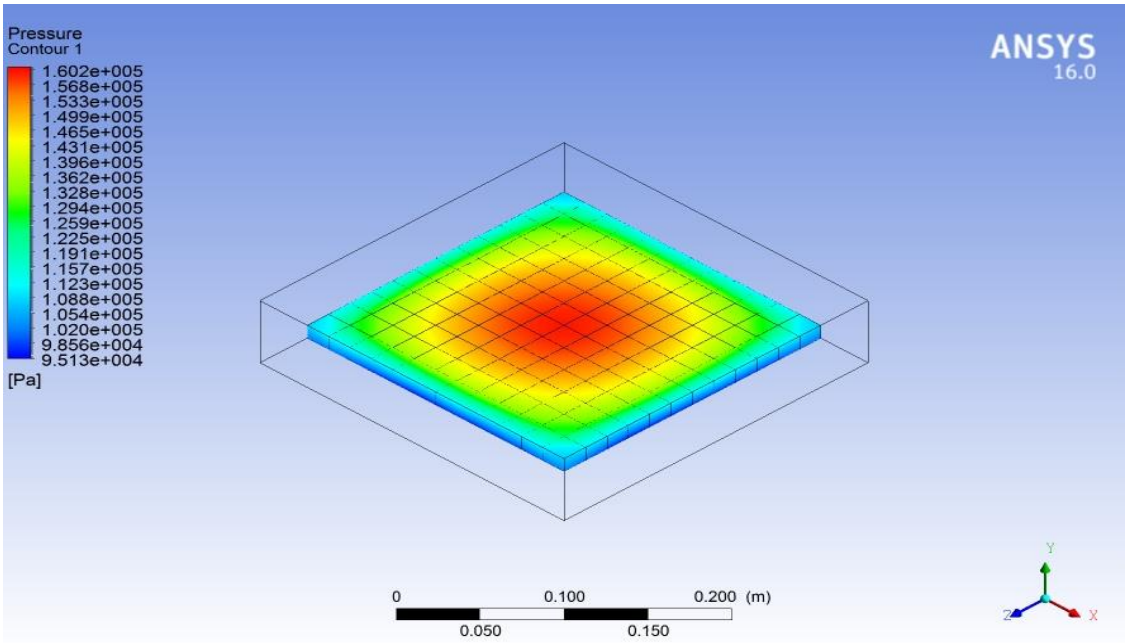

Fig. 8 Pressure variation on the filtration system

The effect of changes in the fluid inlet velocity on the shear stress force of the wall and the distribution of turbulence throughout the filtration results is examined as shown in Tables 6 and 7.

Table 6 The effect of fluid inlet velocity on shear stress of the wall

Velocity (m/s)	**Maximum shear stress of filtration system (Pa)**
20	**7.042**
30	**14.01**
45	**17.02**
60	**19.16**
75	**25.23**

Table 7 The effect of fluid inlet velocity on turbulence distribution in the filtration system

Velocity (m/s)	**Maximum turbulence in the filtration system**
20	**34.16**
30	**39.85**
45	**47.94**
60	**60.46**
75	**84.12**

As can be seen in Tables 6 and 7, by increasing the inlet velocity of the fluid, due to the increase in pressure on the filter located in its middle section and the cross-section of the filter is constant, it increases the force on the filter, which this force increases turbulence throughout the filtration head. To better understand the difference between pressure and temperature distribution in both non-adiabatic and adiabatic modes, Table 8 shows the maximum and minimum values of pressure and temperature distribution on fibrous fibers in both adiabatic and non-adiabatic modes.

As can be seen in Table 8, the pressure on the filtration system itself in the adiabatic state is greater than that for the non-adiabatic state and the temperature in the non-adiabatic state on this system is greater than that for the adiabatic state. It can be said that the pressure on the wall in the non-adiabatic state was higher than that of the adiabatic state and the temperature on it in the adiabatic state was higher than that for the non-adiabatic state.

In the final part of the analysis, the use of different insulation coatings with different thicknesses on the wall around the filtration system is studied and the coefficient of conductivity is evaluated. Consequently, the effect of using each of the three different coatings with the behavioral characteristics of each is presented in Table 9. Table 10 shows the comparison of the results of the lowest and highest heat transfer coefficients of coatings

Table 8 Comparison of pressure and temperature in both adiabatic and non-adiabatic cases

Section	Type of the analysis	Maximum Temperature (K)	Minimum Temperature (K)	Maximum Pressure (Pa)	**Minimum Pressure (Pa)**
Filtration System	Adiabatic	9.864×10^{2}	1.074×10^{3}	1.609×10^{5}	**1.049×10^{5}**
	Non-adiabatic	1.606×10^{5}	8.111×10^{2}	1.606×10^{5}	**1.074×10^{5}**
Around Wall	Adiabatic	1.099×10^{3}	1.052×10^{3}	1.363×10^{5}	**1.966×10^{5}**
	Non-adiabatic	7.584×10^{2}	3.387×10^{2}	1.941×10^{5}	**1.381×10^{5}**

Table 9 Specifications of the desired coatings

Coatings kind	Thermal Conductivity Factor (W/m. K)	Thermal Capacity (J/Kg. K)	Density (Kg/m^3)
SiO_2	1.5	730	2650
Sic	20.7	650	3250
Si_3N_4	43	1100	2650

Table 10 Comparison of the results of the lowest and highest heat transfer coefficients of coatings

Material / Heat Transfer Factor	Max. Heat Transfer Factor $[Wm^{-2}K^{-1}]$	Min. Heat Transfer Factor $[Wm^{-2}K^{-1}]$
SiO_2	3.463×10^{4}	5.137×10^{3}
sic	5.311×10^{4}	7.124×10^{3}
Si_3N_4	5.804×10^{4}	7.537×10^{3}

Since the use of SiO2 coating has the lowest heat transfer coefficient, it creates the highest resistance and the lowest heat loss in the system, resulting in the highest efficiency of the filtration system. The optimal thickness of each coating is examined to prevent heat loss and improve system efficiency. Eleven different thicknesses ranging from 0 to 1.5 mm are examined to determine the optimal thickness for each coating. The optimal coating thickness for SiO2 is 1 mm, for SiC is 1.2 mm, and for Si3N4 is 1.4 mm. With these optimal thickness values, SiO2 coating provides the most effective insulation, resulting in prevention of 19.34% of system losses. The performance of each coating can be evaluated based on heating time with temperature changes, as shown in Fig. 9 where each coating has a thickness of 1 mm. It can be observed that the performance of SiO2 coating is better than that of the

other two coatings, confirming its high performance in terms of heat transfer coefficient and achieving the highest efficiency in the filtration system. There is a sharp increase in heating time up to 300 s, after which the slope of the diagrams decreases. Increasing thickness results in lower heat loss from 0 to 1 mm, but beyond that range, heat loss remains unchanged.

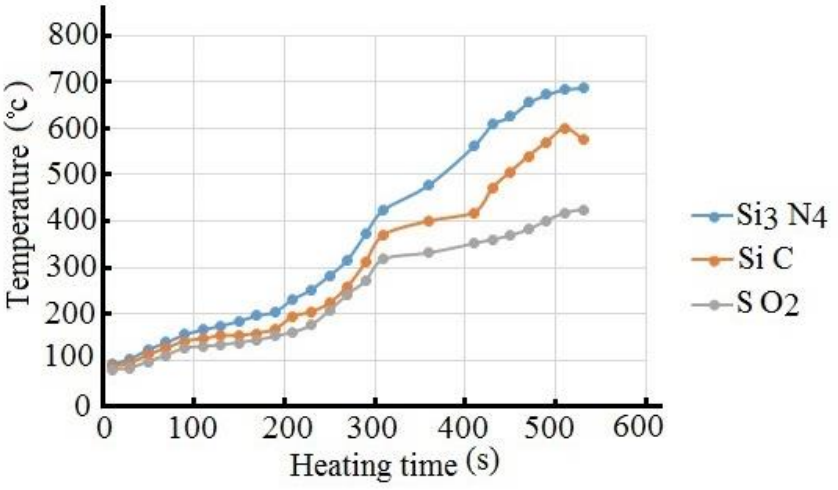

(A)

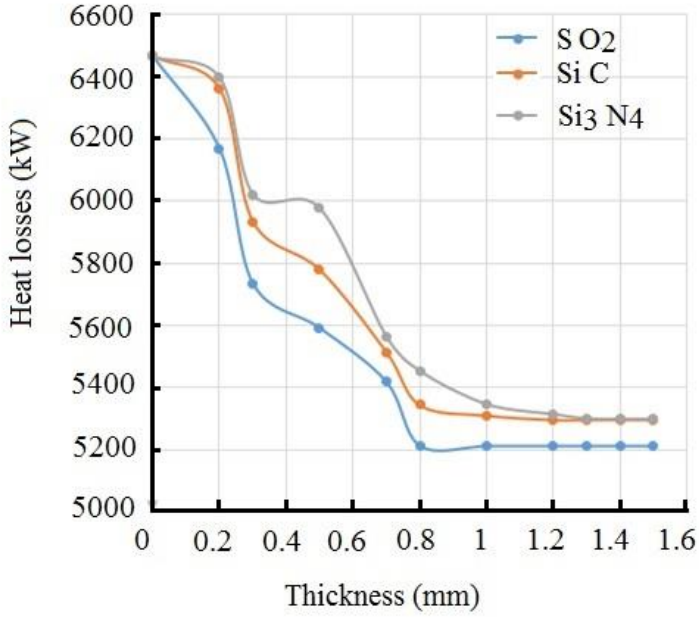

(B)

Fig. 9 Comparison of temperature changes and thickness of coating on heating time (A) and heat losses (B) in the proposed filtration system.

5. Conclusion

In this paper, three-dimensional modeling of a fiber filter with random fibers has been performed to investigate the effect of Brownian and thermophoresis forces on nanoparticle filtration within this filter's environment. After examining and analyzing mesh independence and determining optimal network dimensions, the k-ε viscosity model is used to examine forces on the filtration system and surrounding walls.

- The results related to pressure changes, fluid velocity changes in the system, turbulence coefficient, and coverage around the filtration system are studied under both adiabatic and non-adiabatic conditions to evaluate their effect on system efficiency. With increasing fluid velocity and angle of attack on the system, pressure on the filter increases along with force on the system. Examining fluid inlet velocity changes from 20 to 75 m/s reveals that force on system fibers increases due to increased pressure on the middle section where the filtration system is located, leading to increased turbulence throughout the entire system.
- It can be seen from the pressure contours that the pressure in the middle side of filtration is the highest due to the accumulation of nanoparticles, with a maximum value of 160 kPa. This is while the pressure in the corners of filtration has the lowest value of 95.13 kPa.
- Kinetic energy and shear stress of the wall behave similarly to each other and directly affect each other. In

other words, as the shear stress of the wall increases, the kinetic energy of the fluid will also increase, which can affect the turbulence of the fluid. The issue that distinguishes this study from similar research is the type of chamber insulation coating around the nanoparticle filtration system to prevent energy loss. In other words, this research focuses on different methods and types of nanoparticle filtration system coating. In addition, by considering the type of coating, other important benefits such as increasing the efficiency of the system were also considered. However, it should be noted that in some special cases, these coatings suffer disappearance, in which case, the base material (under the coating) is exposed to hot gases.

- The effect of insulation coatings on the wall of the automation system is investigated in order to prevent high heat transfer. So, we used three types of coatings: SiO2, SiC, and Si3 N4. The results showed that the optimal thickness for SiO2 is 1 mm, SiC is 1.2 mm, and Si3 N4 is 1.4 mm. Results show that SiO2 reduces energy losses to 19.34%. In other words, the desired thickness for all three types of coatings differs due to differences in their performance, and each prevents a drop in different efficiencies.

6. Recommendation for future works

The condition of the system in case of damage or destruction of the coating must be carefully checked in future studies to continue preparing a coating that eliminates these defects well. It is recommended to study different economic aspects of proposed models and evaluate them for use in drug delivery science. Additionally, studying using proposed models for removing extra particles from refrigerants used in the gas processing industry can be explored in future research

Nomenclature

Symbols	
C	Nanoparticle concentration
D_m	Mobility diameter (nm)
P	Pressure (kPa)
T	Temperature ($^{\circ}\mathrm{C}$)
μ	Dynamic viscosity (Pa s)
k	Heat conduction coefficient (W/mK)
ρ	Density (kg/m3)
k_d	Boltzmann constant
f	Volume force
V	Velocity (m/s)

References

Cha, Minju, Chanhee Boo, and Chanhyuk Park. 2022. "Simultaneous Retention of Organic and Inorganic Contaminants by a Ceramic Nanofiltration Membrane for the Treatment of Semiconductor Wastewater." *Process Safety and Environmental Protection* 159:525–33. doi: 10.1016/j.psep.2022.01.032.

Chen, Shaowei, Peng Liu, Zhenchun Li, Ning Tang, Tianwei Li, Yunwu Yu, Feihong Li, and Yuanyuan Bi. 2023. "Preparation and Performance of Composite Nanofiltration Membrane Modified by Mussel Coating." *Journal of Polymers and the Environment*. doi: 10.1007/s10924-023-02928-5.

Chen, Yuhao, Haixiang Sun, Sihui Tang, Huimei Feng, Hongbin Zhang, Kuo Chen, Peng Li, and Q. Jason Niu. 2022. "Nanofiltration Membranes with Enhanced Performance by Constructing an Interlayer Integrated with Dextran Nanoparticles and Polyethyleneimine Coating." *Journal of Membrane Science* 654. doi: 10.1016/j.memsci.2022.120537.

Cheng, Yung Sung, Yuji Yamada, and Hsu Chi Yeh. 1990. "Diffusion Deposition on Model Fibrous Filters with Intermediate Porosity." *Aerosol Science and Technology* 12(2). doi: 10.1080/02786829008959347.

Faramarzi, S., R. Ghasemiasl, and F. Ghadami. 2021. "Numerical Investigation of the Impact of Inclined Baffles and an Elastic Vibrating Beam on the Thermo-Fluid Behavior in a Rectangular Channel." *SN Applied Sciences* 3(5). doi: 10.1007/s42452-021-04568-7.

Gozálvez-Zafrilla, J. M., and A. Santafé-Moros. 2010. "Implementation of the DSPM Model Using a Commercial Finite Element System." *Desalination* 250(2). doi: 10.1016/j.desal.2008.11.053.

Hayat, Tasawar, Muhammad Ijaz Khan, Muhammad Waqas, and Ahmed Alsaedi. 2017. "Mathematical Modeling of Non-Newtonian Fluid with Chemical Aspects: A New Formulation and Results by Numerical Technique." *Colloids and Surfaces A: Physicochemical and Engineering Aspects* 518. doi: 10.1016/j.colsurfa.2017.01.007.

Hosseini, S. A., and H. Vahedi Tafreshi. 2010. "Modeling Particle Filtration in Disordered 2-D Domains: A Comparison with Cell Models." *Separation and Purification Technology* 74(2). doi: 10.1016/j.seppur.2010.06.001.

Jiang, Qin, Ziyu Liu, and Sui Zhao. 2022. "Preparation of Tannic Acid-Dopamine Coating Nanofiltration Membrane for Dye Separation." *Guocheng Gongcheng Xuebao/The Chinese Journal of Process Engineering* 22(1). doi: 10.12034/j.issn.1009-606X.221041.

Kashiwada, Shosaku. 2006. "Distribution of Nanoparticles in the See-through Medaka (Oryzias Latipes)." *Environmental Health Perspectives* 114(11). doi: 10.1289/ehp.9209.

Kefayati, G. H. R. 2015. "FDLBM Simulation of Magnetic Field Effect on Mixed Convection in a Two Sided Lid-Driven Cavity Filled with Non-Newtonian Nanofluid." *Powder Technology* 280. doi: 10.1016/j.powtec.2015.04.057.

Kreyling, W. G., M. Semmler, F. Erbe, P. Mayer, S. Takenaka, H. Schulz, G. Oberdörster, and A. Ziesenis. 2002. "Translocation of Ultrafine Insoluble Iridium Particles from Lung Epithelium to Extrapulmonary Organs Is Size Dependent but Very Low." *Journal of Toxicology and Environmental Health - Part A* 65(20). doi: 10.1080/00984100290071649.

Landfahrer, Martin, Rene Prieler, Bernhard Mayr, Hannes Gerhardter, Ronald Schöngrundner, Jürgen Klarner, and Christoph Hochenauer. 2017. "Development of a Numerically Efficient CFD Model to Predict

Transient Temperature Distribution of Mother Tubes Moving Translative and Rotative through a Gas Fired Furnace." *Applied Thermal Engineering* 123. doi: 10.1016/j.applthermaleng.2017.05.093.

Lee, Handol, Doris Segets, Sebastian Süß, Wolfgang Peukert, Sheng Chieh Chen, and David Y. H. Pui. 2017. "Liquid Filtration of Nanoparticles through Track-Etched Membrane Filters under Unfavorable and Different Ionic Strength Conditions: Experiments and Modeling." *Journal of Membrane Science* 524. doi: 10.1016/j.memsci.2016.11.023.

Lim, Seungho, Hyunseol Park, and Weon Gyu Shin. 2017. "Experimental Investigation and Numerical Modeling of the Orientation Angle of Silver Nanowires Passing through Polyester Filters." *Aerosol Science and Technology* 51(3). doi: 10.1080/02786826.2016.1258113.

Lin, Wenqian, Ruifang Shi, and Jianzhong Lin. 2022. "Heat Transfer and Pressure Drop of Nanofluid with Rod- like Particles in Turbulent Flows through a Curved Pipe." *Entropy* 24(3). doi: 10.3390/e24030416.

Razavi, Seyed Esmail, Tohid Adibi, and Saman Faramarzi. 2020. "Impact of Inclined and Perforated Baffles on the Laminar Thermo-Flow Behavior in Rectangular Channels." *SN Applied Sciences* 2(2). doi: 10.1007/s42452-020-2078-8.

Sheikholeslami, M., and Houman B. Rokni. 2017. "Numerical Modeling of Nanofluid Natural Convection in a Semi Annulus in Existence of Lorentz Force." *Computer Methods in Applied Mechanics and Engineering* 317. doi: 10.1016/j.cma.2016.12.028.

Tang, Ping, Daihong Kuang, Shenghong Yang, and Yueli Zhang. 2016. "Structural, Morphological and Multiferroic Properties of the Hydrothermally Grown Gadolinium (Gd) and Manganese (Mn) Doped Sub-Micron Bismuth Ferrites." *Journal of Alloys and Compounds* 656. doi: 10.1016/j.jallcom.2015.10.010.

Thongyen, Thunyapat, Mitsuhiko Hata, Akira Toriba, Takuji Ikeda, Hiromi Koyama, Yoshio Otani, and Masami Furuuchi. 2015. "Development of PM0.1 Personal Sampler for Evaluation of Personal Exposure to Aerosol Nanoparticles." *Aerosol and Air Quality Research* 15(1). doi: 10.4209/aaqr.2014.05.0102.

Weyd, Marcus, Christian Pflieger, Andy Vogel, Hannes Richter, Volker Prehn, Christiane Günther, Frank Splittgerber, Alessa Gäbler, Daniel Kaulbars, Patrick Bräutigam, Marcus Franke, Samira Lambertz, Julian Schlechtweg, and Ingolf Voigt. 2021. "Removal of Trace Substances with Ceramic Nanofiltration Membranes as Rotating Disk Filters." *Chemie-Ingenieur-Technik* 93(9):1432–39. doi: 10.1002/cite.202100050.

Yadav, Diksha, Sachin Karki, and Pravin G. Ingole. 2022. "Current Advances and Opportunities in the Development of Nanofiltration (NF) Membranes in the Area of Wastewater Treatment, Water Desalination, Biotechnological and Pharmaceutical Applications." *Journal of Environmental Chemical Engineering* 10(4). doi: 10.1016/j.jece.2022.108109.

Zhang, Tong, Hideaki Takahashi, Mitsuhiko Hata, Akira Toriba, Takuji Ikeda, Yoshio Otani, and Masami Furuuchi. 2017. "Development of a Sharp-Cut Inertial Filter Combined with an Impactor." *Aerosol and Air Quality Research* 17(2). doi: 10.4209/aaqr.2016.07.0293.